

Stability of Ice/Rock Mixtures with Application to a Partially Differentiated Titan

Joseph G. O'Rourke, David J. Stevenson

*Division of Geological and Planetary Sciences,
California Institute of Technology, Pasadena, CA 91125, USA*

Abstract

Titan's moment of inertia, calculated assuming hydrostatic equilibrium from gravity field data obtained during the Cassini-Huygens mission, implies an internal mass distribution that may be incompatible with complete differentiation. This suggests that Titan may have a mixed ice/rock core, possibly consistent with slow accretion in a gas-starved disk, which may initially spare Titan from widespread ice melting and subsequent differentiation. A partially differentiated Titan, however, must still efficiently remove radiogenic heat over geologic time. We argue that compositional heterogeneity in the major Saturnian satellites indicates that Titan formed from planetesimals with disparate densities. The resulting compositional anomalies would quickly redistribute to form a vertical density gradient that would oppose thermal convection. We use elements of the theory of double-diffusive convection to create a parameterized model for the thermal evolution of ice/rock mixtures with a stabilizing compositional gradient. To account for large uncertainties in material properties and accretionary processes, we perform simulations for a wide range of initial conditions. Ultimately, for realistic density gradients, double-diffusive convection in the ice/rock interior can delay, but not prevent, ice melting and differentiation, even if a substantial fraction of potassium is leached from the rock component. Consequently, Titan is not partially differentiated.

Keywords: Titan, interior; Saturn, satellites; Jupiter, satellites; Thermal histories

1. Introduction

Titan is Saturn's largest satellite, the second largest in our Solar System. The surface of Titan features stable liquid methane/ethane lakes, a hydrocarbon precipitation cycle comparable to Earth's hydrology, and myriad additional geologic features such as dune fields and mountainous terrain (Jaumann et al., 2009). From an astrobiology perspective, Titan is interesting as a modern analogue for pre-biotic Earth (Raulin et al., 2009). Titan has a thick nitrogen atmosphere, which must be sustained by the continuous production of methane (Atreya et al., 2006). Methane may be stored subsurface or perhaps more deeply in stable clathrate-hydrates along with other volatiles and episodically outgassed when internal heating causes melting (Gautier and Hersant, 2005; Tobie et al., 2006). Understanding Titan's fascinating surface, atmosphere, and chemistry requires knowledge of the evolution of its interior.

Measurements of the gravity field of Titan can place indirect constraints on the current structure of its interior. Titan's gravity harmonics were determined to degree 3 through careful tracking of the Cassini spacecraft during four flybys (Iess et al., 2010). The calculated ratio J_2/C_{22} is consistent with the value of 10/3 that is itself consistent with a gravity field dominated by a nearly hydrostatic quadrupole, although non-zero values of other degree 2 and 3 coefficients indicate that nonhydrostatic features are present. If hydrostatic equi-

librium is assumed, however, then Titan's moment of inertia (MoI) factor is found to be $C \sim 0.34$. Here, the MoI is $CM_s R_s^2$, where M_s and R_s respectively represent the mass and radius of Titan. Measurement of the tidal Love number k_2 from additional flybys reveals a relatively large response of the gravity field to the Saturnian tidal field, indicating the presence of a global, subsurface ocean (Iess et al., 2012). The decoupling of Titan's shell from its interior with an ocean may also explain Titan's long-wavelength topography (Nimmo and Bills, 2010), spin pole orientation (Bills and Nimmo, 2011), and Schumann resonance (Simoes et al., 2012).

The $2\text{-}\sigma$ error on J_2/C_{22} is about 3%, centered on 10/3 and dominated by the error in J_2 , according to Iess et al. (2010). We can write $J_2 = J_{2,h} + J_{2,nh}$ and likewise $C_{22} = C_{22,h} + C_{22,nh}$, where "h" means hydrostatic and "nh" means non-hydrostatic. So, $J_{2,h}/C_{22,h}$ is *exactly* 10/3. If the non-hydrostatic parts were completely uncorrelated (i.e., if they did not cancel in the ratio J_2/C_{22}), then the closeness of the observed value to 10/3 is highly significant and precludes a substantial error in MoI. If, on the other hand, the non-hydrostatic parts tend to be correlated (as they would, for example, in the tidal heating model of Nimmo and Bills (2010) or if Titan has undergone True Polar Wander to the preferred orientation of the non-hydrostatic part of the MoI), then the small deviation away from 10/3 does not guarantee smallness of the non-hydrostatic part and the

MoI is accordingly uncertain. The effects of the non-hydrostatic components on Titan’s MoI are explored in detail in Gao and Stevenson (2013). Given the observed power in degree 3 gravity, Iess et al. (2010) propose that the MoI could be as low as 0.33 and we adopt this as a plausible lower bound. The true MoI is likely to be smaller than 0.34, the value inferred from J_2/C_{22} , because this is a lower rotational energy state. Since a fully differentiated Titan may allow 0.33 (but perhaps not 0.34), the differentiation state of Titan is accordingly not yet determined from observation.

Titan’s MoI can be compared to previous results regarding other icy satellites. In particular, Titan’s MoI coefficient is intermediate to the previously-measured $C \sim 0.31$ for Ganymede (Anderson et al., 1996a) and $C \sim 0.35$ for Callisto (Anderson et al., 2001), where hydrostatic equilibrium was assumed *a priori* for the Galilean satellites. While Ganymede is easily modeled as a differentiated satellite with an iron core under a rock shell and an outer ice layer (e.g., Sohl et al., 2002), models of a differentiated Callisto are not consistent with the reported MoI (e.g., Anderson et al., 2001). A proposed interior structure for Callisto features a rock/ice core with rock mass fraction near the close packing limit, with an overlying icy mantle that was depleted of rock by Stokes settling (Nagel et al., 2004). In this case, an ice/rock lithosphere in which density decreases with depth overlays the icy mantle.

Titan might represent an intermediate case between differentiated Ganymede and undifferentiated Callisto. However, the inferred (and widely cited) partially differentiated state for Callisto is based on a gravity inversion that *assumes* $J_2/C_{22} = 10/3$, and perhaps the inferred MoI is incorrect. As for Titan, the sense of the error is likely to cause an overestimate of the MoI because non-hydrostatic contributions to J_2 and C_{22} are likely positive. At present, we cannot exclude the possibility that *all* large icy satellites are fully differentiated. (In this paper, we use that term to imply the complete separation of ice from rock; the further differentiation of an iron core from the rock is a separate issue that we do not address.) It should be noted that non-hydrostatic effects are more likely to be important in slowly rotating bodies (Titan and Callisto) relative to Ganymede because the hydrostatic effects scale as rotational frequency squared for both tides and synchronous rotation (Gao and Stevenson, 2013). Certainly, Callisto and Ganymede are different in appearance and Callisto, like Titan, lacks a global magnetic field.

Relative differences in the experienced intensity of the Late Heavy Bombardment (LHB) may explain the Ganymede/Callisto dichotomy. In the so-called “Nice model,” the gas giant planets swiftly realigned once Jupiter and Saturn crossed their mean motion resonance ~ 700 Myr after planetary formation, quickly causing the outward migration of Uranus and Neptune and the evolution of Jupiter and Saturn’s orbital eccentricities (Tsiganis et al., 2005). The ensuing destabilization of the planetesimal disk and the asteroid belt

caused the LHB of both the outer and inner solar system (Gomes et al., 2005). Ganymede is closer to Jupiter than Callisto, so it likely suffered considerably more high-energy impacts during the LHB. For assumptions about the planetesimal disk consistent with the Nice model, the differences in received energy during the LHB are sufficient to cause Ganymede to differentiate, while Callisto’s rock and ice components may remain unmixed (Barr and Canup, 2010). If Titan survived both accretion and the LHB without melting the ice in its deep interior, then it could have remained partially differentiated like Callisto, at least initially.

Gas giant satellites like Titan were accreted from the outskirts of the disk of material surrounding their parent planets. Nascent gas giant planets must accrete enough rock such that they can also accumulate large amounts of gas, principally hydrogen and helium, before the dissipation of the protoplanetary disk, which had a lifetime of a few Myr (e.g., Lissauer and Stevenson, 2007; Lunine et al., 2009). In the core-nucleated gas accretion model, for instance, the formation of Saturn began with the accretion of km-sized rocky planetesimals from the minimum mass sub nebula (MMSN) (e.g., Lissauer and Stevenson, 2007). However, if gas giant satellites accreted from the outskirts of a disk of planet-forming material as dense and gas-rich as the MMSN, then Jupiter’s Galilean satellites (and, by analogy, Titan) would have formed quickly and hot and therefore differentiated. Additionally, recent work suggests that collisional mergers of Galilean-like satellites may have formed Titan (Asphaug and Reufer, 2013), which would have caused complete differentiation.

Internal structure models for Titan often assume widespread ice melting and thus differentiation. Many studies investigated the thermal evolution of Titan assuming a large silicate/iron core (e.g., Sohl et al., 2003; Tobie et al., 2005), before MoI data from Iess et al. (2010) cast doubt on such models. Papers invoked convection in a silicate core to melt clathrate hydrates and cause episodic outgassing of methane (e.g., Tobie et al., 2006). Another class of models assumes that Titan contains a large core of hydrated silicates, chiefly the serpentine mineral antigorite (Fortes et al., 2007; Grindrod et al., 2008; Castillo-Rogez and Lunine, 2010; Fortes, 2012; Tobie et al., 2012). Serpentinization of silicates in icy satellites is likely to be rapid in the presence of liquid water, e.g. during differentiation or subsequent hydrothermal convection (Ransford et al., 1981; Travis and Schubert, 2005), because the serpentinization reaction promotes crack formation and increasing material permeability (MacDonald and Fyfe, 1985). An interior dominated by hydrated silicates is consistent with constraints on Titan’s chemical evolution (e.g., Fortes et al., 2007; Fortes, 2012). But a partially differentiated Titan, in which Titan’s deep interior is a mixture of ice and rock, is still consistent with the gravity data (Iess et al., 2010) and such models have not been fully vetted.

The accretion of undifferentiated icy satellites is often assumed to occur in a “gas-starved” disk, where

material similar to that found in the gas giant’s feeding zone is fed to the accretion process over millions of years. The resultant, long timescales for satellite accretion allow many of the Galilean satellites, particularly Callisto, to avoid complete differentiation (e.g., Canup and Ward, 2002). In another model, the major satellites of Jupiter and Saturn formed in a solid-enhanced minimum mass planetary nebula, avoiding differentiation as satellites opened gaps in the nebula (Mosqueira and Estrada, 2003a,b). With a particular compositional gradient in the initial circumplanetary disc, the compositions of the major Saturnian satellites can be roughly reproduced (Mosqueira et al., 2010). In any model, accretion must also be delayed to escape intense, but short-lived, radiogenic heating from the decay of ^{26}Al and ^{60}Fe if an icy satellite is to avoid complete differentiation (e.g., McKinnon, 1997; Barr and Canup, 2008). Despite myriad threats to unmelted ice, slow accretion in a gas-starved disk permits the formation of a partially differentiated Titan (Barr et al., 2010).

The purpose of this study is to determine whether a partially differentiated Titan is stable over geologic time. After accretion, the internal ice/rock mixture must efficiently expel radiogenic heat, which would otherwise melt the ice and allow irreversible sinking and separation of the rock component. Because the major Saturnian satellites are remarkably heterogeneous, we argue that Titan likely accreted from planetesimals with disparate rock mass fractions. Even without that heterogeneity, there may be a tendency to form a stably stratified interior at the outset. Soon after accretion, a stabilizing density gradient would be established in which rock mass fraction increases with depth. Aspects of the theory of double-diffusive convection allow us to formulate a one-dimensional, parameterized thermal evolution model in which a convecting layer slowly grows to encompass the entire ice/rock interior. We perform simulations for a large set of initial conditions because of uncertainties in key parameters and to analyze the sensitivity of our results. Finally, we discuss alternatives to a partially differentiated Titan and consider possible implications for other icy satellites.

2. Theoretical formulation

Our simple model assumes that Titan is a sphere of radius R_s and mass M_s , consisting of an undifferentiated ice/rock interior with radius R_i and an overlying shell. The structure of the outer shell may be complicated, especially considering the likely presence of an ocean, but we do not need to model it in detail. We perform parametrized thermal evolution simulations to assess whether Titan can remain partially differentiated until the present. Stabilizing compositional gradients, caused by increasing rock mass fraction and thus density with depth, likely inhibit convection in Titan’s ice/rock interior. Elements from the theory of double-diffusive convection are incorporated to model thermal evolution with this complication. Although this simple

model will not precisely reconstruct the thermal history of Titan, it does provide a first-order test of the hypothesis of partial differentiation.

2.1. Establishment of vertical density gradients

The major Saturnian satellites exhibit significant compositional heterogeneity. The average densities of each satellite vary widely, from $\sim 990 \text{ kg m}^{-3}$ for Tethys to $\sim 1,600 \text{ kg m}^{-3}$ for Enceladus (Jacobson, 2004). We can calculate a mass-weighted density:

$$\bar{\rho}_{mw} = \frac{\sum_i m_i \bar{\rho}_i}{\sum_i m_i}, \quad (1)$$

where m_i and $\bar{\rho}_i$ are the masses and mean densities of each satellite, respectively. Considering the eight major satellites excluding Titan (Mimas, Enceladus, Tethys, Dione, Rhea, Hyperion, Iapetus, and Phoebe), $\bar{\rho}_{mw} \approx 1,270 \text{ kg m}^{-3}$ (Jacobson, 2004). Titan’s mean density is $\sim 1,881 \text{ kg m}^{-3}$, but its uncompressed density is not much higher than the densities of the other Saturnian satellites. In fact, the inner satellites (the first five of the aforementioned) and Saturn’s almost-pure water ice rings may have been formed from tidal stripping of a Titan-sized satellite that was lost within Saturn’s classical Roche limit (Canup, 2010).

Since Titan was plausibly formed from planetesimals of size and composition similar to these satellites, lateral density anomalies as large as 10% likely existed after accretion. These unstable anomalies drive a flow that will restructure the ice/rock mixtures, so that more dense mixtures underlie less dense mixtures, in a length of time that scales as

$$t_f \sim \frac{\mu}{\Delta\rho_{lat}gD}, \quad (2)$$

where μ is viscosity, $\Delta\rho_{lat}$ is the horizontal density anomaly, g is gravitational acceleration, and D is the length scale of the anomalies. A competing process is the Stokes settling of the dense rock fragments from the ice/rock mixture. Using the usual Stokes settling velocity, the time in which the rock fragments settle out of the mixture scales as

$$t_s \sim \frac{\mu D}{\Delta\rho g R^2}, \quad (3)$$

where $\Delta\rho$ is the density difference between the ice and the rock ($\sim 1,000$ to $2,000 \text{ kg m}^{-3}$) and R is the radius of the rock fragments. For $R \sim 1 \text{ m}$ and $D \sim 100 \text{ km}$, the formation of the vertical density gradients overwhelms the Stokes settling of the rocks if the lateral density anomaly is greater than only one part in ten billion of the density difference between the ice and rock, i.e. $t_f < t_s$ if $\Delta\rho_{lat} > 10^{-10}\Delta\rho$. Clearly, this is easily achieved.

Mixing during accretion will not homogenize the differences arising from large planetesimals. Importantly, lateral differences during the accretion lead to vertical differences in ice/rock ratio after settling, even if individual impact events mix vertically. Therefore, models

of Titan’s thermal evolution must consider the existence of up to $\sim 10\%$ stabilizing density gradients in Titan’s ice/rock interior initially (and even smaller effects are still very important because thermal expansion of ice produces much smaller density differences). A vertical density gradient, where density increases with depth, opposes thermal buoyancy, inhibiting convection and thus militating against substantial heat transfer. If radiogenic heat is not removed from the system, then the ice in Titan’s deep interior will melt, especially if low melting point components such as ammonia are present. The liberated rock components will sink as the melt percolates upwards. Runaway differentiation can occur if the gravitational energy released by the sinking of the rock component is sufficient to melt more ice (Friedson and Stevenson, 1983), but complete differentiation may occur without invoking runaway differentiation if convection is sufficiently suppressed.

2.2. Double-diffusive convection applied to Titan

The theory of double-diffusive convection was originally developed to elucidate various phenomena in oceanography (Stern, 1960). In general, double-diffusive phenomena occur in the presence of two opposing density gradients when the two responsible components have different molecular diffusivities (e.g., Turner, 1974). The theory has been extended to the dynamics of magma chambers and stellar interiors (e.g., Spiegel, 1972; Schmitt, 1983; Turner, 1985), but remains most often utilized in oceanography. For instance, in Earth’s high latitudes, the polar oceans are composed of cold, fresh water overlying warm, salty water (e.g., Schmitt, 1994). In the presence of the stabilizing salinity gradient, convective motions resembling Rayleigh-Bénard convection arise after a stage of steady oscillating motions in layers cooled from above (Veronis, 1968; Noguchi and Niino, 2010). These well-mixed, convecting layers increase in thickness and frequently merge with neighboring layers of equal density. This is known as the “diffusive-layer” mode, in which salinity, the stabilizing component, has a much lower molecular diffusivity than temperature, the component driving convection.

Titan’s deep interior features analogous opposing temperature and compositional gradients. The compositional gradient is simply a measure of the increasing rock mass fraction in the ice/rock mixture with depth. Although a temperature gradient can induce particle motion through interfacial premelting (Rempel et al., 2001), the relevant time scales are far too long for application to icy satellites. Hence, the molecular diffusivity associated with the rock component is effectively zero. Because the molecular diffusivity of salt is non-zero, in contrast, complicated temperature and salinity profiles exist in the ocean (e.g., Huppert and Turner, 1981), with time-dependent fluxes of salt and temperature across diffusive interfaces between the multiple convecting layers (e.g., Worster, 2004). Regardless, the term “double-diffusive” is still applicable to our model

of convection in the presence of a stabilizing gradient. As outlined below, aspects of the theory applied to Titan do not depend on the molecular diffusivity of the component opposing temperature.

In Titan, double-diffusive convection occurs in the presence of a stabilizing rock mass fraction gradient as its deep interior is cooled from above and heated from within. The density within the ice/rock interior is a linear function of rock mass fraction and temperature (Turner, 1974):

$$\rho = \rho_0(1 - \alpha\Delta T + \beta\Delta S), \quad (4)$$

where ρ_0 is the density at some reference depth, α is the coefficient of thermal expansion, and $\beta = (1/\rho)(\partial\rho/\partial S)_T$ is the coefficient of compositional expansion, analogous to α , associated with the change in rock mass fraction. The change of density due to pressure alone can be omitted because it does not contribute to the convective stability and is in any event too small to greatly affect the form of the convective motions. Table 1 contains numerical values of these coefficients and other constants used in this study. The rock mass fraction may be calculated (Barr et al., 2010):

$$S = \frac{\rho_r(\bar{\rho} - \rho_i)}{\bar{\rho}(\rho_r - \rho_i)}, \quad (5)$$

where $\bar{\rho}$ is the average density, ρ_r is the density of rock, and ρ_i is the density of ice. High-pressure ice phases V, VI, and VII may exist within Titan’s deep interior; a representative density $\rho_i = 1,400 \text{ kg m}^{-3}$ is chosen in accord with Barr et al. (2010). Although the mineralogy of Titan’s rock component is not completely known, CI carbonaceous chondrites and Prinn-Fegley rock, an assemblage that models condensate from the proto-Jovian nebula, are possible analogues, motivating the choice $\rho_r = 3,300 \text{ kg m}^{-3}$ (Mueller and McKinnon, 1988; Barr et al., 2010).

A quick calculation with Eqs. 4 and 5 reveals why compositional gradients make melting much more likely in a partially differentiated Titan. A $\sim 10\%$ density contrast across Titan’s interior corresponds to $\Delta S \sim 10^{-1}$ between ice/rock parcels at the top and bottom of the mixture. So, an (impossible) temperature increase of $\Delta T \sim 10^3 \text{ K}$ is required before compositionally dense parcels can become buoyant.

For cooling from above and heating from within, but with the top temperature kept constant, convection begins at the top of Titan’s ice/rock interior. The onset of convection must occur at an upper thermal boundary layer because the temperature gradient throughout the ice/rock interior is initially adiabatic. With a linear density distribution, an equation for a measure of the initial stability gradient may be written (Turner, 1973):

$$N_S^2 = -g\beta\frac{dS}{dz}, \quad (6)$$

where N_S is a frequency of oscillation. When heat flows out of the top of the convecting layer, the associated

Constant	Definition	Value	Units	Ref.
A	Activation parameter for ice	25	-	[1]
κ	Thermal diffusivity	10^{-6}	$\text{m}^2 \text{s}^{-1}$	[1]
α	Coefficient of thermal expansivity	10^{-4}	K^{-1}	[1]
β	Coefficient of compositional expansivity	1.1	-	*
M_s	Mass of Titan	1.345×10^{23}	kg	[2]
R_s	Radius of Titan	2575	km	[2]
R_i	Radius of ice/rock interior	2000	km	*
ρ_i	Density of ice	1400	kg m^{-3}	[2]
ρ_r	Density of rock	3300	kg m^{-3}	[2]
$C_{p,i}$	Specific heat of ice	2100	$\text{J kg}^{-1} \text{K}^{-1}$	[2]
$C_{p,r}$	Specific heat of rock	900	$\text{J kg}^{-1} \text{K}^{-1}$	[3]

Table 1: List of key model constants. References: 1. Friedson and Stevenson (1983), 2. Barr et al. (2010), 3. Grindrod et al. (2008), *this study.

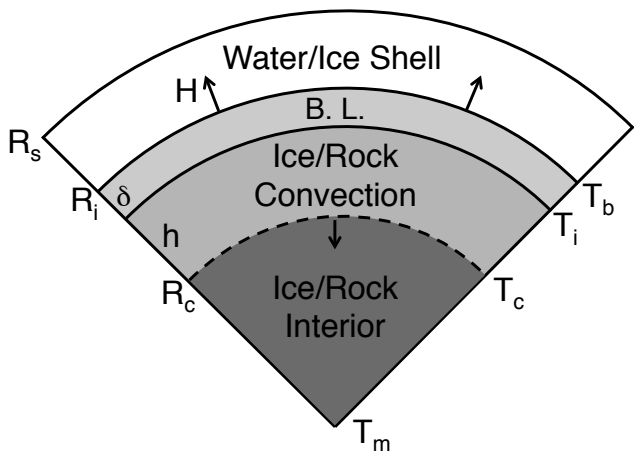


Figure 1: Cartoon showing the assumed structure of Titan after the initialization of double-diffusive convection in the interior ice/rock region, before the convecting layer has grown to encompass the entire interior. Dimensions are not to scale and the overlying water/ice shell is not drawn in detail. Key model parameters are indicated as used in the text.

buoyancy flux may be calculated (Turner, 1973):

$$B = -\frac{g\alpha H}{\rho C_p}. \quad (7)$$

As cooling continues from above, a well-mixed convecting layer grows with height (Turner, 1973):

$$h = \left(\frac{2Bt}{N_S^2}\right)^{1/2}. \quad (8)$$

Therefore, the rate of the growth of the convecting layer may be calculated:

$$\frac{dh}{dt} = \left[\frac{\alpha H}{2\rho C_p \beta (dS/dz)t}\right]^{1/2}. \quad (9)$$

Figure 1 shows the internal structure of Titan after double-diffusive convection has proceeded for some time. The radius of the ice/rock interior is R_i . The non-convecting ice/rock core has radius R_c , where T_c and T_m respectively represent the outer and inner temperatures.

A thermal boundary layer exists between the convecting outer shell and the convecting ice/rock interior with thickness δ . The temperature at the top of the thermal boundary layer, T_b , is held constant, while the temperature of the convecting layer is T_i . Parametrized thermal evolution models typically assume adiabatic temperature gradients in convecting layers, but these temperature increases with depth are negligible.

2.3. Governing equations

Energy in the convecting ice/rock layer is conserved:

$$4\pi R_i^2 H = \frac{4\pi}{3} \bar{\rho} (R_i^3 - R_c^3) \left(Q - C_p \frac{dT_i}{dt} \right) - \rho_i f_i L_m, \quad (10)$$

where H is the heat flux out of the convecting ice/rock layer into the overlying shell, Q is radiogenic heat production, f_i is the volume of melted ice, and L_m is the latent heat of melting. The specific heat of the ice/rock mixture is a mass-weighted average (Barr and Canup, 2008):

$$C_p = S C_{p,r} + (1 - S) C_{p,i}, \quad (11)$$

where $C_{p,r}$ and $C_{p,i}$ are the specific heats of the rock and ice components, respectively. Assuming that no melting occurs, we can conveniently rewrite Eq. 10:

$$C_p \frac{dT_i}{dt} = Q - \frac{3H}{\bar{\rho}} \frac{R_i^2}{R_i^3 - R_c^3}. \quad (12)$$

We consider contributions to radiogenic heat production from ^{40}K , ^{235}U , ^{238}U , and ^{232}Th . Radiogenic heating in the ice/rock mixture may be calculated (e.g., Barr and Canup, 2008):

$$Q(t) = S \sum_n c_{n,0} P_{n,0} \exp(-\lambda_n t), \quad (13)$$

where, for the n th isotope, $c_{n,0}$ is the initial abundance, $P_{n,0}$ is the initial specific heat production, and λ_n is the decay constant. Table 2 lists the constants used to calculate radiogenic heat production.

With this formulation, $t = 0$ Gyr in Eq. 13 corresponds to the formation of the calcium-aluminum-rich inclusions (CAIs) in chondrites. If Titan formed exactly

Isotope	$c_{n,0}$ [ppb]	$P_{n,0}$ [$\mu\text{W}/\text{kg}$]	λ_n [1/Gyr]
^{238}U	16.91	93.7	0.155
^{235}U	5.275	569	0.985
^{232}Th	38.71	26.9	0.0495
$^{40}\text{K} \rightarrow ^{40}\text{Ar}$	813.8	1.02	0.0581
$^{40}\text{K} \rightarrow ^{40}\text{Ca}$	813.8	26.69	0.4962

Table 2: Constants used to calculate radiogenic heat production, adapted from Barr and Canup (2008).

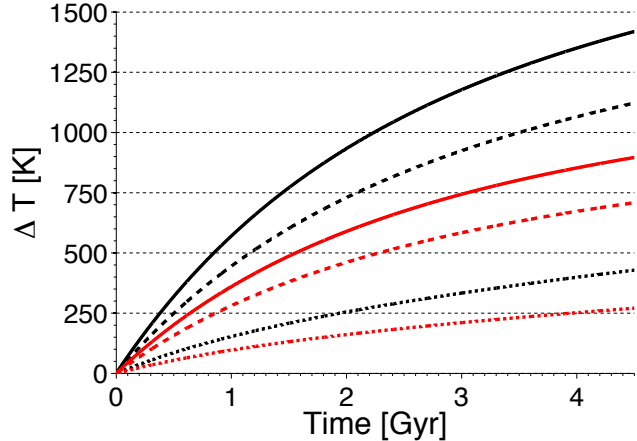


Figure 2: Temperature increase in a parcel of rock (black, $S = 1.0$) and in an ice/rock mixture with $S = 0.8$ (red). Solid, dashed, and dotted lines respectively represent $f = 1.0, 0.7,$ and 0.3 .

coincident with the CAIs, however, intense heating from ^{26}Al and ^{60}Fe would have caused widespread melting and hence differentiation (e.g., Barr et al., 2010). We implicitly assume that, in reality, Titan accreted several Myr after the formation of the CAIs and thus we may ignore these short-lived isotopes. A delay of a few Myr barely changes the amount of radiogenic heating from ^{40}K , ^{235}U , ^{238}U , and ^{232}Th . Because we do not aim to precisely constrain the timing of Titan’s accretion, we simply repeat our simulations starting at $t_0 = 5$ and 10 Myr to confirm that our results do not change appreciably. Note that heating from ^{26}Al and ^{60}Fe would only lower the chances of survival for a partially differentiated Titan.

Because contact between silicates and ammonia/water liquid can leach volatile ^{40}K out of the rock component (e.g., Engel et al., 1994), we multiply the initial abundance of potassium by f , a depletion factor. Figure 2 shows representative temperature increases over 4.5 Gyr for $S = 1.0$ and 0.8 from radiogenic heat production with $f = 1.0, 0.7,$ and 0.3 .

2.4. Thermal evolution of Titan’s ice/rock interior

A one-dimensional parametrized model can simulate the thermal evolution of the ice/rock mixture within Titan. The viscosity of the ice/rock mixture is a critical parameter, subject to large uncertainty. Although the deformation of ice is non-Newtonian under the conditions of Titan’s deep interior, an Arrhenius-like equation may suffice for low strain rates (Friedson and

Stevenson, 1983):

$$\eta = \frac{\nu_0}{\rho} \exp \left[A \left(\frac{T_m}{T} - 1 \right) \right], \quad (14)$$

where A is an activation parameter and T_m is the melting point of water ice, calculated using data from Petrenko and Whitworth (1999). For conditions appropriate to icy satellites, adding rock particles to a water ice matrix may cause viscosity to increase by an order of magnitude (Friedson and Stevenson, 1983), but we do not explicitly model these effects in this study.

At first, a conductive boundary layer grows with thickness $\delta \sim \sqrt{\kappa t}$ at the top of the ice/rock interior. The conductive heat flux out of the boundary layer is

$$H = \frac{k\Delta T}{\delta}, \quad (15)$$

where $k = \kappa\rho C_p$ is thermal conductivity and κ is thermal diffusivity. The initial growth of the conductive boundary layer stops and convection begins when the Rayleigh number for the boundary layer reaches a critical value, i.e.,

$$Ra_c = \frac{g\alpha\Delta T\delta_c^3}{\eta(T)\kappa} = 10^3, \quad (16)$$

where ΔT is the temperature contrast across the boundary layer and δ_c is the critical thickness of the boundary layer.

After convection begins, the viscosity contrast between the convecting ice/rock mixture and the overlying shell of high pressure ice is less than the ~ 4 orders of magnitude required to produce a stagnant lid. So, the heat flux is given by the following equation (Friedson and Stevenson, 1983):

$$H = 0.1k(\Delta T)^{4/3} \left[\frac{g\alpha}{\eta(T_i)\kappa} \right]^{1/3}, \quad (17)$$

where $\Delta T = T_b - T_i$ is the temperature contrast driving convection. The thickness of the thermal boundary layer, δ , can be calculated using the condition for convective instability

$$\frac{g\alpha\Delta T\delta_i^3}{\eta(T_i - 0.5\Delta T)\kappa} = 10^3. \quad (18)$$

In reality, the thermal evolution of the ice shell above the thermal boundary layer is complicated. Titan likely has a shell consisting of an outer ice I layer, an ocean, and a mantle of high-pressure ice polymorphs (e.g., Iess et al., 2012). Convection in the ice I shell is expected for small grain sizes (Barr and McKinnon, 2007; Mitri and Showman, 2008), but the long-wavelength topography of Titan implies shell thickness variations that convection might eliminate, indicating that Titan’s ice I shell may be currently conductive (Nimmo and Bills, 2010). Possibly, part of this shell is clathrate hydrate, which has different transport properties. If the mantle of high-pressure ice is convecting, then a system of

equations, for the convective instability of and temperature contrasts across the thermal boundary layers at the interface with the ice/rock interior, is necessary to precisely calculate the thermal evolution of Titan. Because our focus is on the thermal evolution of Titan’s deep interior, we assume for simplicity that T_b is constant in all simulations.

3. Numerical models

We performed simulations to calculate the thermal history of Titan’s ice/rock interior for 4.5 Gyr. The model described above was numerically iterated with a time step of 1 Myr. Internal temperatures were compared to the phase diagram for pure water ice from Petrenko and Whitworth (1999) at each time step to determine whether melting occurs. Titan, as a whole, has $\bar{\rho} = 1,881 \text{ kg m}^{-3}$ and $S \approx 0.44$. We assume that Titan is initially composed of an outer shell with a thickness of 575 km and a density of $1,200 \text{ kg m}^{-3}$. Therefore, $R_i = 2,000 \text{ km}$ and $S \approx 0.82$ in the ice/rock interior. The average density of the ice/rock interior, $\bar{\rho} = 2,653 \text{ kg m}^{-3}$. In this simple two-layer model, the normalized moment of inertia coefficient $C \approx 0.343$. The melting temperatures of water ice are ~ 280 and 500 K at pressures of ~ 0.7 and 4.7 GPa , respectively, which are the conditions at the top and bottom of the ice/rock interior.

A wide parameter space was explored by varying the initial conditions for hundreds of simulations. The temperature at the top of the thermal boundary layer in the ice/rock interior was fixed at $T_b = 200 \text{ K}$, but we used both $T_m(0) = 200$ and 125 K to explore the effects of different initial temperature gradients, as suggested by models of Titan’s accretion (Mitri et al., 2010). Initial rock mass fraction gradients were imposed that produced effective density changes throughout the ice/rock interior as large as $\Delta\rho_s \sim 0.1\bar{\rho}$ (i.e., $\sim 10\%$). An initial temperature gradient, if present, also produces an effective density change of $\Delta\rho_t \sim \alpha\Delta T_i$, where $\Delta T_i = T_b - T_m(0)$. In some simulations, no initial compositional gradient was imposed. Because of the large uncertainty on the viscosity of ice/rock mixtures, we tested effective viscosities near melting in the range $\nu_0 = 10^{11}$ to 10^{15} Pa s . (Even larger values increase the likelihood of melting and lower values are much lower than physically plausible.) To account for the possibility of potassium leaching and uncertainties in the rock mineralogy, we conducted simulations using three different depletion factors: $f = 1.0, 0.7, \text{ and } 0.3$. Guided by the results of these simulations, we construct some plausible present-day internal structure models for Titan.

4. Results

The following sections summarize the results of our simulations, beginning with the presentation of four representative thermal histories. Next, we discuss the effects of various initial conditions using a large number of simulation results. Finally, simulations in which

melting occurred are analyzed to determine the details of melting in the ice/rock interior.

4.1. Sample thermal histories

Four examples of calculated thermal histories are shown in Fig. 3. In each simulation, a convecting layer with constant temperature grows over time, eventually encompassing the entire ice/rock interior. From 2.5 to 4.5 Gyr, this convecting ice/rock layer cools monotonically. Underneath the convecting layer, temperatures increase from radiogenic heating, although the initial linear temperature gradient is preserved. The internal temperature profile must be continuous; our model implies the existence of thermal boundary layers on both sides of the conductive/convective interface. These relatively thin layers are neither explicitly modeled nor depicted in Fig. 3. No melting occurs in any of these four examples within 4.5 Gyr because the convecting layer grows fast enough to encompass the entire interior before temperatures in the non-convecting layer increase enough to cause widespread melting and differentiation.

Comparisons between pairs of these simulations illuminate the effects of varying the magnitude of compositional gradients, potassium depletion, and initial temperature gradients. Simulations shown in panels A and B, for instance, both have $f = 1.0$, $\nu_0 = 10^{14} \text{ Pa s}$, and $T_m(0) = 125 \text{ K}$. Panel A features a $\sim 1\%$ compositional gradient, i.e., $\Delta\rho_s = 0.01\bar{\rho}$, whereas the initial density gradient in panel B is only the result of the initial temperature gradient. The growth of the convecting layer is relatively delayed by $\sim 500 \text{ Myr}$ in panel A, allowing an additional $\sim 100 \text{ K}$ of heating in the ice/rock interior.

Panels A and C illustrate the effects of potassium depletion on the thermal evolution of an ice/rock interior with a $\sim 1\%$ compositional gradient. All initial conditions are identical for both simulations, except $f = 0.3$ in panel C. The primary effect of potassium depletion is to slow the growth of the convecting layer because heating in the underlying, non-convecting layer is necessary to overcome the initial compositional gradient. Specifically, convection in the entire ice/rock interior is delayed by $\sim 1.25 \text{ Gyr}$. The maximum temperatures reached in the non-convecting ice/rock interior, however, are only slightly lower in panel C than in panel A. On the other hand, the temperature of the convecting layer is generally reduced in panel C, since the convecting layer is relatively thin, internal heating is lessened, and the incorporation of hot material from the non-convecting interior is more gradual.

Finally, panels C and D reveal the effects of varying the effective viscosity near melting. Both simulations include substantial potassium depletion ($f = 0.3$) and start with a $\sim 1\%$ compositional gradient. While panel C features $\nu_0 = 10^{14} \text{ Pa s}$ as usual, $\nu_0 = 10^{12} \text{ Pa s}$ in panel D. With a lower viscosity, the convecting layer has a lower temperature and takes slightly longer to encompass the entire interior. In fact, convecting layer growth is faster for the first $\sim 500 \text{ Myr}$ in panel D, but marginally slower thereafter. Thus, heat flux out of

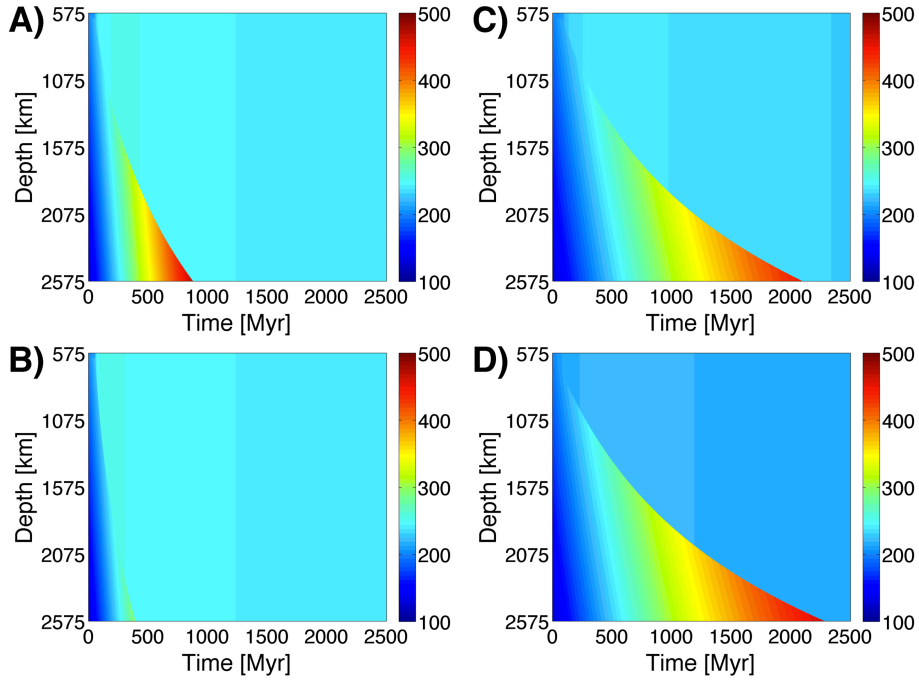


Figure 3: Representative results for simulations in which melting did not occur. Temperature profiles in Titan’s ice/rock interior are plotted until the time after which the convecting interior cools monotonically. The thermal boundary layers on either side of the conductive/convective interface are neither modeled nor shown. Default initial conditions for the four simulations are $T_b = 200$ K, $T_m(0) = 125$ K, $f = 1$, $\log_{10}(\nu_0) = 14$, and $\Delta\rho_s = 0.01\bar{\rho}$. Panel B has $\Delta\rho_s = 0$. Panel C has $f = 0.3$. Panel D has $f = 0.3$ and $\log_{10}(\nu_0) = 12$.

the convecting layer is relatively low after a period of relatively rapidly cooling and convecting layer growth. Compared to the other initial conditions, however, the sensitivity of the model to uncertainties in viscosity is very small.

4.2. Sensitivity to initial conditions

Figure 4 shows results from 810 simulations of the thermal evolution of Titan’s ice/rock interior. The purpose of each panel is to illustrate whether or not melting occurs for a particular set of initial conditions. Horizontal axes indicate the range of density differences across the ice/rock interior induced by an initial compositional gradient, i.e., $\Delta\rho_s = 0$ to $0.03\bar{\rho}$. Each vertical axis represents a range of effective viscosities near melting, i.e., $\nu_0 = 10^{11}$ to 10^{15} Pa s. Blue circles signify simulations in which melting never occurred, whereas red squares represent simulations where widespread melting would have caused differentiation of Titan’s ice/rock interior within 4.5 Gyr.

Each panel represents a series of simulations that started with different initial temperature gradients and magnitudes of potassium depletion. The top and bottom rows of panels, for instance, have $T_m(0) = 125$ and 200 K, respectively. In general, melting is less likely to occur without an initial temperature gradient, because a temperature decrease with depth induces a density gradient that suppresses convection. High-viscosity simulations with low compositional gradients in panels D and E feature melting, while the corresponding

simulations in panels A and B do not. The lack of a significant density gradient from compositional or temperature changes in these simulations causes the convecting layer to very quickly encompass the interior, homogenizing internal temperatures. Because the average internal temperature is comparatively high at first, however, melting occurs near the top of the ice/rock interior, where melting temperatures are relatively low.

Figure 4 also elucidates the effects of potassium depletion. From left to right, columns of panels have $f = 1.0$ (A and D), 0.7 (B and E), and 0.3 (C and F). Reducing the abundance of potassium in the rock component of the ice/rock interior only makes melting marginally less likely. As seen in the example thermal histories, potassium depletion only lengthens the time scales on which temperatures increase; the maximum temperatures reached in ice/rock interior are barely lessened. For any plausible choice of initial conditions, melting occurs if the initial compositional gradient is larger than $\sim 2\%$.

4.3. When and where melting occurs

Figure 5 contains more information about 173 simulations in which melting occurred for initial compositional gradients ranging from 1 to 10%. Specifically, panel A illustrates the time at which melting occurred and panel B shows the value of R_c , the radius of the non-convecting ice/rock interior, at the time when melting began. As in Fig. 4, six different sets of initial conditions were used. That is, black and red symbols respectively

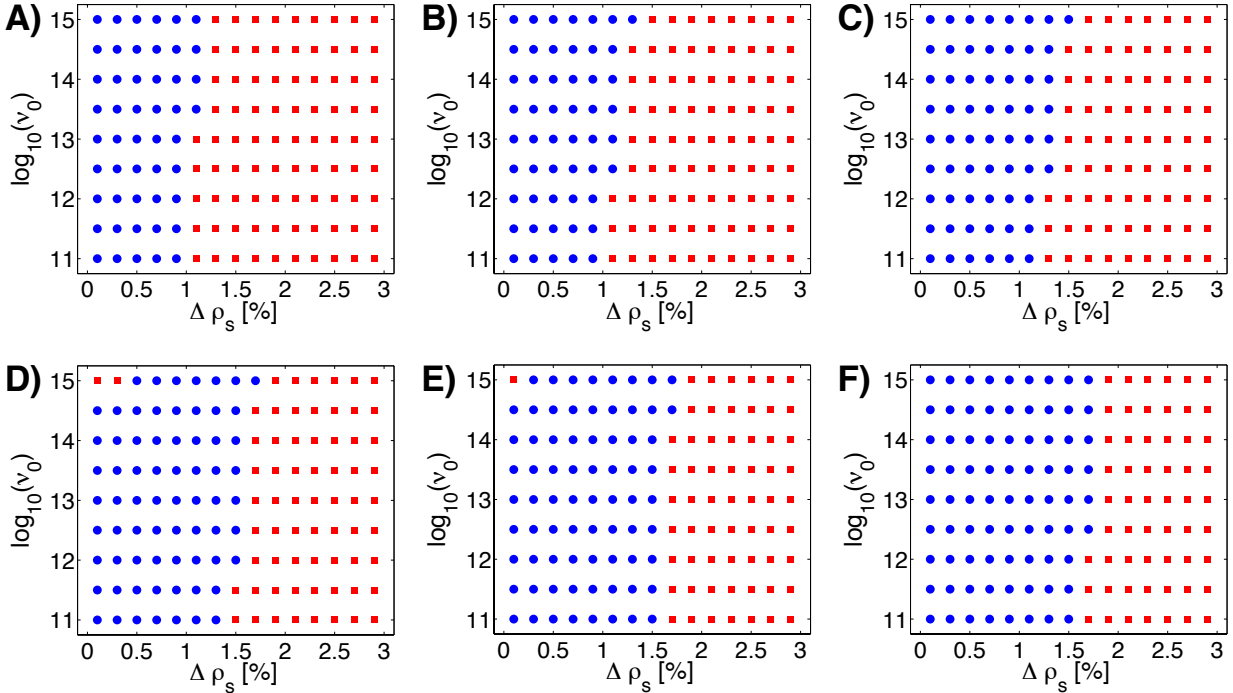


Figure 4: Sensitivity analyses results for 810 simulations exploring the effects of potassium depletion, effective viscosity near melting, and initial temperature and compositional gradients. In each panel, the horizontal axis shows the total density variation across the ice/rock interior produced by the initial compositional gradient. The vertical axes show the dynamic viscosity near melting assumed for each simulation. Blue circles represent simulations in which no melting occurred in 4.5 Gyr; red squares signify simulations in which melting occurred at any point in the ice/rock interior. All simulations have $T_b = 200$ K. From left to right, each column of panels features $f = 1.0, 0.7,$ and 0.3 . The top and bottom rows of panels have $T_m(0) = 125$ and 200 K, respectively. For initial compositional gradients producing $\Delta\rho_s > 0.02\bar{\rho}$, melting occurs during all simulations.

represent $T_m(0) = 125$ and 200 K. For circular, square, and triangular markers, respectively, $f = 1.0, 0.7,$ and 0.3 . With large density gradients, the non-convecting ice/rock core always melts before the ice in the convecting layer.

The magnitudes of potassium depletion and the initial temperature gradient more strongly affect when melting occurs than where it begins. That is, increasing potassium depletion can delay melting by ~ 500 Myr to 1.75 Gyr for a given initial compositional gradient, but the radius of the non-convecting core at the time when melting begins only slightly decreases. With no initial temperature gradient but a higher average internal temperature, melting occurs sooner, but the convecting layer has grown further before melting begins. As compositional gradients increase, melting occurs sooner, the convecting layer is thinner when melting occurs, and the simulation’s sensitivity to the choice of initial conditions decreases. Beginning the simulations at $t_0 = 5$ or 10 Myr after the origin of the CAIs delayed the onset of melting by $\ll 100$ Myr.

5. Discussion

5.1. Stability of a partially differentiated Titan

A partially differentiated Titan is stable over geologic time if it can safeguard the ice in its deep interior from widespread melting caused by radiogenic heating. If

thermal convection is vigorous throughout the entire ice/rock layer, then melting can be avoided. Even for small compositional gradients ($\sim 1-1.5\%$) a convecting layer can grow to encompass the entire ice/rock interior before internal temperature profiles cross the melting curve of water ice. Larger compositional gradients ($\sim 5-10\%$), however, are plausible since Titan likely accreted from heterogeneous planetesimals. Thermal buoyancy simply cannot overcome these stabilizing gradients without causing ice melting and complete differentiation. The likely presence of ammonia in the ice component, which may significantly lower the melting temperature (e.g., Loveday et al., 2009), compounds the problem.

No plausible selection of initial conditions allows sufficiently efficient heat removal in the presence of a large compositional gradient. A substantial amount of heat-producing ^{40}K may be leached out of the rock component through contact with liquid water or ammonia-water solutions. Roughly 30% of the original abundance of potassium has been estimated to have been extracted from the silicates of Ganymede (Kirk and Stevenson, 1987) and Titan (Engel et al., 1994), and almost complete leaching of several elements has been suggested for Enceladus (Glein and Shock, 2010). A reduction in the magnitude of radiogenic heating may be important to preventing Titan’s interior from reaching temperatures associated with silicate dehydration (Castillo-Rogez and Lunine, 2010), but, as seen in

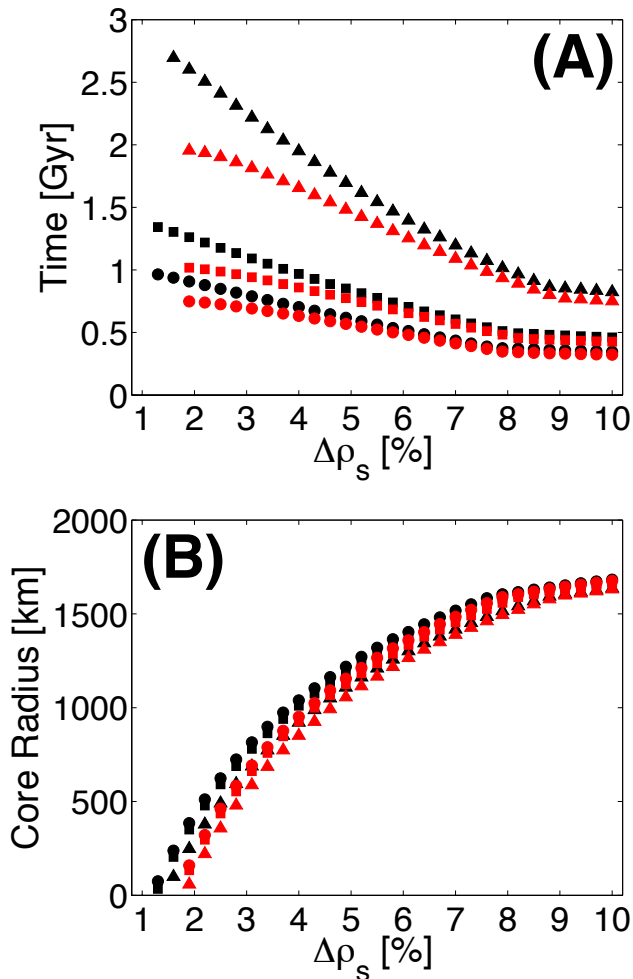


Figure 5: Details of melting during 186 simulations of Titan’s thermal evolution with initial compositional gradients that produce density contrasts from $0.01\bar{\rho}$ to $0.1\bar{\rho}$ across the ice/rock interior. Panel A shows when melting occurs in the non-convecting ice/rock interior. Panel B illustrates the size of the non-convecting ice/rock core at the time when melting occurs. All simulations have $T_b = 200$ K. Black and red symbols respectively represent $T_m(0) = 125$ and 200 K. Circular, square, and triangular markers represent $f = 1.0, 0.7,$ and $0.3,$ respectively.

Fig. 2, any plausible abundance of radioisotopes, even with $\sim 70\%$ leaching of ^{40}K , will eventually produce enough heat to melt ice. Crucially, internal heating drives the growth of the double-diffusive convecting layer, so potassium depletion suppresses the initialization of convection throughout the entire ice/rock interior.

Double-diffusive convection involves opposing gradients of two components that have different diffusivities. With components like salt and water, both diffusivities are non-zero, and multiple convecting layers form. In Titan’s ice/rock system, however, the diffusivity of the rock component is effectively zero, and we only model the growth of a single layer. For small compositional gradients, the time scale for the growth of a convective instability of a new layer is much greater the time scale on which the first layer grows. With sufficiently large compositional gradients, growth of the convecting

layer is slow enough that additional layers could form if melting never occurred, but melting typically occurs in ~ 250 to 750 Myr. In any case, heat transport through a series of convecting layers is comparatively inefficient (e.g., Turner, 1974), and the formation of many layers is unlikely to prevent complete differentiation.

5.2. Alternative internal structures

A partially differentiated Titan is a non-unique interpretation of available gravity data (Iess et al., 2010). Because Titan’s ice/rock interior is unstable to differentiation over geologic time, alternate models should be considered. One popular hypothesis is that Titan’s interior is chiefly composed of hydrated silicates (e.g., Fortes et al., 2007; Castillo-Rogez and Lunine, 2010; Fortes, 2012). Three serpentine polymorphs are typically found in carbonaceous chondrites: chrysotile, lizardite, and antigorite. Antigorite is the most abundant, and its properties are usually used to track the thermochemical evolution of model assemblages (e.g., Castillo-Rogez and Lunine, 2010). After heating melts the ice component of an ice/rock mixture, redistributing rock and melt into a stable density structure with homogenized internal temperatures takes a few hundred Myr (Kirk and Stevenson, 1987; Lunine and Stevenson, 1987). The serpentinization reaction between the liberated silicates and the surrounding liquid would likely proceed to completion well before core overturn is finished (MacDonald and Fyfe, 1985).

Models assuming a core composed entirely of antigorite are missing a significant mass of iron. The formula for the magnesium end-member of antigorite is $\text{Mg}_3\text{Si}_2\text{O}_5(\text{OH})_4$. But Fe^{2+} and Fe^{3+} often substitute into the Mg^{2+} and Al^{3+} sites, respectively, yielding a typical iron number of $\text{Fe}/(\text{Fe}+\text{Mg}) \sim 0.2$ (Scott et al., 2002). That is, antigorite has <14 wt% Fe, significantly less than the ~ 18.2 wt% Fe typically found in CI chondrites (Hutchinson, 2004, p. 29). So, ~ 4 wt% Fe, equivalent to an Fe-rich core with a radius of a few hundred km, must accompany a mass of antigorite created from the serpentinization of silicates with chondritic composition, although some iron may be in soluble form in Titan’s ocean. The presence of a relatively small Fe-rich core does not dramatically affect Titan’s moment of inertia (Castillo-Rogez and Lunine, 2010).

Figure 6 shows two end-member models for the present-day internal structure of Titan for which $C \sim 0.34$. In structure A, Titan is dominated by an hydrated silicate core with $R = 1,950$ km and $\bar{\rho} = 2,700$ kg m^{-3} . An Fe-rich core with $R = 500$ km and $\bar{\rho} = 6,500$ kg m^{-3} , representing ~ 4 wt% of the iron/rock interior is also present, although the formation of an Fe-rich core would likely dehydrate the overlying silicates. The overlying shell, composed of an ice I lid, an ocean, and high-pressure ice polymorphs, is modeled as a single layer with an average density of $1,202$ kg m^{-3} . The lower ~ 300 km of antigorite could be replaced with dehydrated silicates in structure A without decreasing the MoI coefficient below $C \sim 0.332$

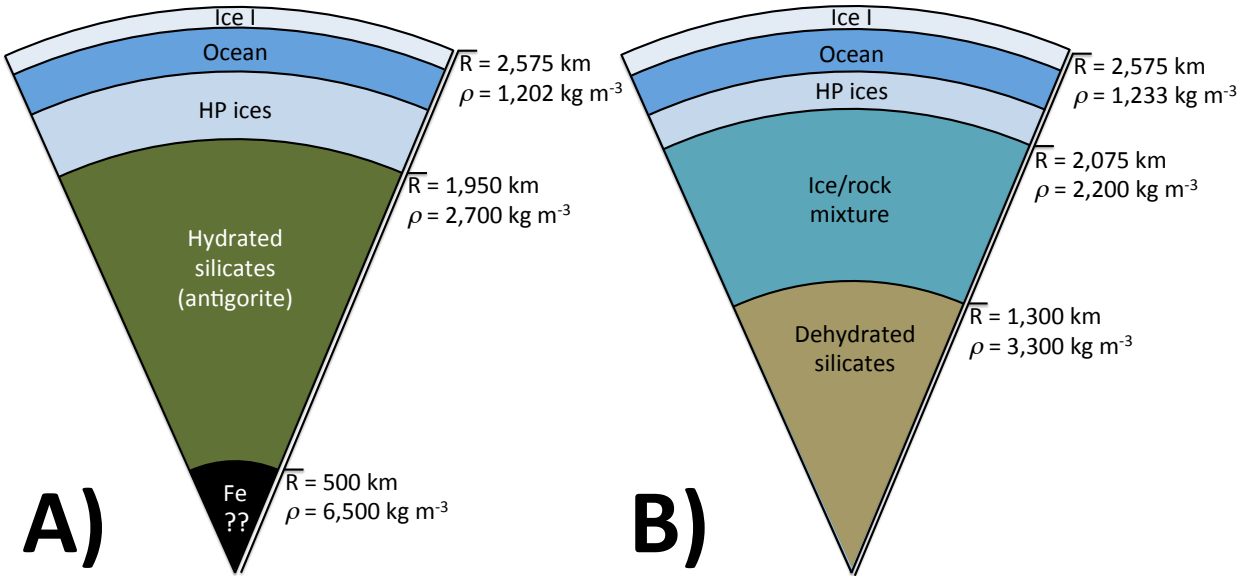


Figure 6: Two end-member internal structures for Titan that have $C \sim 0.34$. Possible material layers include an Fe-rich core, dehydrated silicates, hydrated silicates, and an ice/rock mixture. Each model includes high-pressure ices, a water ocean with dissolved gases and solids, and a layer of water ice I, all of which are modeled as a single shell with constant density. Titan’s atmosphere is neither depicted nor modeled.

A key question is whether significant dehydration of the silicate core should be expected. The equilibrium temperature for the antigorite dehydration reaction is ~ 800 to 900 K for conditions appropriate to Titan (e.g., Perrillat et al., 2005), although dehydration in a water saturated environment may be kinetically hindered and not occur until temperatures reach ~ 1060 K (Seipold and Schilling, 2003), and the heat flux from the advection of warm water could be significant. Castillo-Rogez and Lunine (2010) found that conductive heat transport could delay significant dehydration until very recently, assuming $\sim 30\%$ potassium depletion and a relatively high specific heat for antigorite. Serpentine dehydration at the present may be responsible for melting clathrate hydrates in the overlying ice shell, releasing methane (Tobie et al., 2006) and radiogenic ^{40}Ar (Niemann et al., 2005) onto the surface and into the atmosphere. We suggest that, if Titan formed partially differentiated, double-diffusive convection in the initial ice/rock mixture may have delayed core overturn for as long as ~ 1 Gyr beyond what was assumed in Castillo-Rogez and Lunine (2010), helping the eventual core of hydrated silicates avoid dehydration.

Current data do not exclude partially differentiated models featuring a large silicate core. Structure B in Fig. 6 is an example of such a model, similar to those considered in McKinnon and Bland (2011). An ice/rock mantle with $R = 2,075$ km, $\bar{\rho} = 2,200$ kg m $^{-3}$, and $S \sim 0.63$ overlies a core of dehydrated silicates with $R = 1,300$ km and $\bar{\rho} = 3,300$ kg m $^{-3}$. A decreased rock mass fraction and a smaller length scale for the ice/rock layer might allow efficient convection, even in the presence of a stabilizing compositional gradient. Evaluating the thermal stability of such a structure would require coupling the thermal evolution of all three lay-

ers, potentially including the effects of tidal dissipation, as has been done for Ganymede (Bland et al., 2009). More complicated variations on structure B featuring different ice/rock mixtures or a hydrated portion of the silicate core are also valid interpretations of the gravity data. Differences in the predicted tidal responses of these two models may allow discrimination between these two alternatives (Castillo-Rogez and Lunine, 2012).

5.3. Implications for other icy satellites

Gravity measurements by spacecraft suggest a spectrum of internal structures for the icy satellites of Jupiter and Saturn. The formation of an undifferentiated or a partially differentiated satellite requires a sequence of conditions: slow accretion in a gas-starved disk, delayed to avoid catastrophic heating from the radioactive decay of short-lived isotopes, and then survival of intense impacts from the Late Heavy Bombardment (Barr and Canup, 2008, 2010; Barr et al., 2010). The Radau-Darwin approximation is primarily used to calculate the MoI of a satellite with the measured J_2 and C_{22} coefficients, but a unique solution only exists for a satellite in hydrostatic equilibrium.

Non-hydrostatic structures in the degree 2 gravity of Titan may introduce significant inaccuracies into the Radau-Darwin approximation (Gao and Stevenson, 2013). Indeed, Iess et al. (2010) reported non-hydrostatic geoid height variations as large as 19 m for Titan, possibly indicating that Titan’s MoI coefficient could be closer to that of Ganymede than earlier reported. The measured MoI for Callisto is likewise subject to large uncertainties because of possible non-hydrostatic effects, which are not excluded by current

data (Anderson et al., 2001), but an equivalent departure from hydrostatic equilibrium would have a relatively small effect on Ganymede. The Galilean satellites are not as compositionally heterogeneous as the major Saturnian satellites (Anderson et al., 1996b,a, 1998, 2001), so the likelihood of substantial compositional gradients suppressing convection in Callisto may be lessened. In any case, the radio science instrument on the planned *JUICE* (JUpiter ICy moons Explorer) mission may allow the vastly improved measurement of the gravity fields of Ganymede and Callisto and thus the identification of gravity anomalies and significant non-hydrostatic features. With these new data, we may continue to vet the spectrum of internal differentiation states proposed for icy satellites.

The internal structures of Saturn’s medium-sized satellites may also shed light on the formation and evolution of the Saturnian system. Unfortunately, their MoIs are not yet tightly constrained. Gravity data from the Cassini mission suggest that Rhea, Saturn’s second-largest satellite, has a larger MoI coefficient than Titan (Iess et al., 2007). Based on a preliminary analysis, Anderson and Schubert (2007) claimed that Rhea’s interior was a homogenous ice/rock mixture (i.e., with no compositional gradient). Further analysis indicates that rock must be at least somewhat concentrated towards the center of Rhea (Iess et al., 2007), perhaps in a core with relatively high rock mass fraction, even if Rhea’s gravity field is subject to significant non-hydrostatic effects (Mackenzie et al., 2008). The rock mass fraction of Rhea is almost half that of Titan, so a relative scarcity of radiogenic heating may stave off differentiation. The simple model developed in this paper for Titan may not be directly applicable to Rhea, which is much smaller than Titan, but future thermal evolution simulations would help evaluate whether the proposed internal structures are plausible.

6. Conclusions

Titan can survive accretion and the Late Heavy Bombardment without suffering complete differentiation if it formed slowly in a gas-starved disk, and a partially differentiated Titan is consistent with recently obtained gravity data. But radiogenic heating tends to melt ice in the undifferentiated interior over geologic time, causing irreversible sinking of the rock component. If the ice/rock interior is initially homogenous, then thermal convection may remove sufficient heat to prevent melting. Two sources of compositional gradients, however, act to suppress convection. First, Titan likely had a temperature profile immediately after accretion in which temperature decreased with depth. Second, accretion from heterogeneous planetesimals would produce a stabilizing rock mass fraction gradient, where rock mass fraction and thus density increased with depth. Convection in the presence of opposing compositional and thermal gradients is “double-diffusive”, comprising a convecting layer that slowly grows from the top

of the ice/rock interior. For compositional gradients larger than a few percent, this convecting layer does not grow fast enough to prevent widespread melting in the non-convecting core. A partially differentiated Titan is therefore unstable over geologic time. The general instability of ice/rock mixtures with compositional gradients may have significant consequences for other icy satellites.

7. Acknowledgments

J.G. O’Rourke thanks A.C. Barr, W.B. McKinnon, and I. Mosqueira for helpful discussions and the NASA Planetary Geology & Geophysics Undergraduate Research Program for support. Constructive comments from one reviewer improved the content and clarity of this manuscript. J.G. O’Rourke is supported by a National Science Foundation Graduate Research Fellowship.

8. References Cited

References

- Anderson, J.D., Schubert, G., 2007. Saturn’s satellite Rhea is a homogeneous mix of rock and ice. *Geophys. Res. Lett.* 37, L02202, doi:10.1029/2006GL028100.
- Anderson, J.D., Jacobson, R.A., McElrath, T.P., Moore, W.B., Schubert, G., Thomas, P.C., 2001. Shape, mean radius, gravity field, and interior structure of Callisto. *Icarus* 153, 157–161, doi:10.1006/icar.2001.6664.
- Anderson, J.D., Lau, E.L., Sjogren, W.L., Schubert, G., Moore, W.B., 1996a. Gravitational constraints on the internal structure of Ganymede. *Nature* 384, 541–543.
- Anderson, J.D., Schubert, G., Jacobson, R.A., Lau, E.L., Moore, W.B., Sjogren, W.L., 1998. Europa’s differentiated internal structure: Inferences from four Galileo encounters. *Science* 281, 2019–2022.
- Anderson, J.D., Sjogren, W.L., Schubert, G., 1996b. Galileo gravity results and the internal structure of Io. *Science* 272, 709–712.
- Asphaug, E., Reufer, A., 2013. Late origin of the Saturn system. *Icarus* 223, 544–565, doi:10.1016/j.icarus.2012.12.009.
- Atreya, S.K., Adams, E.Y., Niemann, H.B., Demick-Montelara, J.E., Owen, T.C., Fulchignoni, M., Ferri, F., Wilson, E.H., 2006. Titan’s methane cycle. *Planet. Space Sci.* 54, 1177–1187, doi:10.1016/j.pss.2006.05.028.
- Barr, A.C., Canup, R.M., 2008. Constraints on gas giant satellite formation from the interior states of partially differentiated satellites. *Icarus* 198, 163–177, doi:10.1016/j.icarus.2008.07.004.
- Barr, A.C., Canup, R.M., 2010. Origin of the Ganymede-Callisto dichotomy by impacts during the late heavy bombardment. *Nat. Geosci.* 3, 164–167, doi:10.1038/NNGEO746.
- Barr, A.C., Citron, R.I., Canup, R.M., 2010. Origin of a partially differentiated Titan. *Icarus* 209, 858–862, doi:10.1016/j.icarus.2010.05.028.
- Barr, A.C., McKinnon, W.B., 2007. Convection in ice I shells and mantles with self-consistent grain size. *J. Geophys. Res.* 112, E02012, doi:10.1029/2006JE002781.
- Bills, B.G., Nimmo, F., 2011. Rotational dynamics and internal structure of Titan. *Icarus* 214, 351–355, doi:10.1016/j.icarus.2011.04.028.
- Bland, M.T., Showman, A.P., Tobie, G., 2009. The orbital-thermal evolution and global expansion of Ganymede. *Icarus* 200, 207–221, doi:10.1016/j.icarus.2008.11.016.
- Canup, R.M., 2010. Origin of Saturn’s rings and inner moons by mass removal from a lost Titan-sized satellite. *Nature* 468, 943–946.

- Canup, R.M., Ward, W.R., 2002. Formation of the Galilean satellites: conditions of accretion. *Astronom. J.* 124, 3404–3423.
- Castillo-Rogez, J.C., Lunine, J.I., 2010. Evolution of Titan's rocky core constrained by Cassini observations. *Geophys. Res. Lett.* 37, L20205, doi:10.1029/2010GL044398.
- Castillo-Rogez, J.C., Lunine, J.I., 2012. Tidal response of Titan's interior models consistent with Cassini-derived constraints. *LPSC XLIII Abstracts #1707*.
- Engel, S., Lunine, J.I., Norton, D.L., 1994. Silicate interactions with ammonia-water fluids on early Titan. *J. Geophys. Res.* 99, 3745–3752.
- Fortes, A.D., 2012. Titan's internal structure and the evolutionary consequences. *Planet. Space Sci.* 60, 10–17, doi:10.1016/j.pss.2011.04.010.
- Fortes, A.D., Grindrod, P.M., Trickett, S.K., Vocado, L., 2007. Ammonium sulfate on Titan: Possible origin and role in cryovolcanism. *Icarus* 188, 139–153, doi:10.1016/j.icarus.2006.11.002.
- Friedson, A.J., Stevenson, D.J., 1983. Viscosity of rock-ice mixtures and applications to the evolution of icy satellites. *Icarus* 56, 1–14.
- Gao, P., Stevenson, D.J., 2013. Nonhydrostatic effects and the determination of icy satellites moment of inertia. *Icarus* 226, 1185–1191, doi:10.1016/j.icarus.2013.07.034.
- Gautier, D., Hersant, F., 2005. Formation and composition of planetesimals: Trapping volatiles by clathration. *Space Sci. Rev.* 116, 25–52, doi:10.1007/s11214-005-1946-2.
- Glein, C.R., Shock, E.L., 2010. Sodium chloride as a geophysical probe of a subsurface ocean on Enceladus. *Geophys. Res. Lett.* 37, L09204, doi:10.1029/2010GL042446.
- Gomes, R., Levison, H.F., Tsiganis, K., Morbidelli, A., 2005. Origin of the cataclysmic Late Heavy Bombardment period of the terrestrial planets. *Nature* 435, 466–469, doi:10.1038/nature03676.
- Grindrod, P.M., Fortes, A.D., Nimmo, F., Feltham, D.L., Brodholt, J.P., Vocado, L., 2008. The long-term stability of a possible aqueous ammonium sulfate ocean inside Titan. *Icarus* 197, 137–151, doi:10.1016/j.icarus.2008.04.006.
- Huppert, H.E., Turner, J.S., 1981. Double-diffusive convection. *J. Fluid Mech.* 106, 299–329.
- Hutchinson, R., 2004. *Meteorites. A Petrologic, Chemical and Isotopic Synthesis.* Cambridge University Press.
- Iess, L., Jacobson, R.A., Ducci, M., Stevenson, D.J., Lunine, J.I., Armstrong, J.W., Asmar, S.W., Racioppa, P., Rappaport, N.J., Tortora, P., 2012. The tides of Titan. *Science*, doi:10.1126/science.1219631.
- Iess, L., Rappaport, N.J., Jacobson, R.A., Racioppa, P., Stevenson, D.J., Tortora, P., Armstrong, J.W., Asmar, S.W., 2010. Gravity field, shape, and moment of inertia of Titan. *Science* 327, 1367–1369, doi:10.1126/science.1182583.
- Iess, L., Rappaport, N.J., Tortora, P., Lunine, J., Armstrong, J.W., Asmar, S.W., Somenzi, L., Zingoni, F., 2007. Gravity field and interior of Rhea from Cassini data analysis. *Icarus* 190, 585–593, doi:10.1016/j.icarus.2007.03.027.
- Jacobson, R.A., 2004. The orbits of the major Saturnian satellites and the gravity field of Saturn from spacecraft and Earth-based observations. *Astrophys. J.* 128, 492–501, doi:10.1086/421738.
- Jaumann, R., Kirk, R.L., Lorenz, R.D., Lopes, R.M.C., Stofan, E., Turtle, E.P., Keller, H.U., Wood, C., Sotin, C., Soderblom, L.A., Tomasko, M.G., 2009. Geology and surface processes on Titan, in: Brown, R.H., Lebreton, J.P., Waite, J.H. (Eds.), *Titan from Cassini-Huygens.* Springer. chapter 5.
- Kirk, R.L., Stevenson, D.J., 1987. Thermal evolution of a differentiated Ganymede and implications for surface features. *Icarus* 69, 91–134.
- Lissauer, J.J., Stevenson, D.J., 2007. Formation of giant planets, in: Reipurth, B., Jewitt, D., Keil, K. (Eds.), *Protostars and Planets V.* University of Arizona Press, Tucson, pp. 591–606.
- Loveday, J.S., Nelmes, R.J., Bull, C.L., Maynard-Casely, H.E., Guthrie, M., 2009. Observation of ammonia dihydrate in the AMH-VI structure at room temperature - possible implications for the outer solar system. *High Pressure Res.* 29, 396–404, doi:10.1080/08957950903162057.
- Lunine, J., Choukroun, M., Stevenson, D.J., Tobie, G., 2009. The origin and evolution of Titan, in: Brown, R.H., Lebreton, J.P., Waite, J.H. (Eds.), *Titan from Cassini-Huygens.* Springer. chapter 3.
- Lunine, J.I., Stevenson, D.J., 1987. Clathrate and ammonia hydrates at high pressure: Application to the origin of methane on Titan. *Icarus* 70, 61–77.
- MacDonald, A.H., Fyfe, W.S., 1985. Rate of serpentinization in seafloor environments. *Tectonophysics* 116, 123–135, doi:10.1016/0040-1951(85)90225-2.
- Mackenzie, R.A., Iess, L., Tortora, P., Rappaport, N.J., 2008. A non-hydrostatic Rhea. *Geophys. Res. Lett.* 35, L05204, doi:10.1029/2007GL032898.
- McKinnon, W.B., 1997. Mystery of Callisto: Is it undifferentiated? *Icarus* 130, 540–543, doi:10.1006/icar.1997.5826.
- McKinnon, W.B., Bland, M.T., 2011. Core evolution in icy satellites and Kuiper belt objects. *LPSC XLII Abstracts #2768*.
- Mitri, G., Pappalardo, R.T., Stevenson, D.J., 2010. Evolution and interior structure of Titan. *LPSC XLI Abstracts #2229*.
- Mitri, G., Showman, A.P., 2008. Thermal convection in ice-I shells of Titan and Enceladus. *Icarus* 193, 387–396, doi:10.1016/j.icarus.2007.07.016.
- Mosqueira, I., Estrada, P.R., 2003a. Formation of the regular satellites of giant planets in an extended gaseous nebula I: subnebula model and accretion of satellites. *Icarus* 163, 198–231, doi:10.1016/S0019-1035(03)00076-9.
- Mosqueira, I., Estrada, P.R., 2003b. Formation of the regular satellites of giant planets in an extended gaseous nebula II: satellite migration and survival. *Icarus* 163, 232–255, doi:10.1016/S0019-1035(03)00077-0.
- Mosqueira, I., Estrada, P.R., Charnoz, S., 2010. Deciphering the origin of the regular satellites of gaseous giants — Iapetus: The Rosetta ice-moon. *Icarus* 207, 448–460, doi:10.1016/j.icarus.2009.10.018.
- Mueller, S., McKinnon, W.B., 1988. Three-layered models of Ganymede and Callisto: Compositions, structures, and aspects of evolution. *Icarus* 76, 437–464.
- Nagel, K., Breuer, D., Spohn, T., 2004. A model for the interior structure, evolution, and differentiation of Callisto. *Icarus* 169, 402–412, doi:10.1016/j.icarus.2003.12.019.
- Niemann, H.B., Atreya, S.K., Bauer, S.J., Carignan, G.R., Demick, J.E., Frost, R.L., Gautier, D., Haberman, J.A., Harpold, D.N., Hunten, D.M., Israel, G., Lunine, J.I., Kasprzak, W.T., Owen, T.C., Paulkovich, M., Raulin, F., Raaen, E., Way, S.H., 2005. The abundances of constituents of Titan's atmosphere from the GCMS instrument on the Huygens probe. *Nature* 438, 779–784, doi:10.1038/nature04122.
- Nimmo, F., Bills, B.G., 2010. Shell thickness variations and the long-wavelength topography of Titan. *Icarus* 208, 896–904, doi:10.1016/j.icarus.2010.02.020.
- Noguchi, T., Niino, H., 2010. Multi-layered diffusive convection. Part I. Spontaneous layer formation. *J. Fluid Mech.* 651, 443–464, doi:10.1017/S0022112009994150.
- Perrillat, J.P., Daniel, I., Koga, K.T., Reynard, B., Cardon, H., Crichton, W.A., 2005. Kinetics of antigorite dehydration: A real-time X-ray diffraction study. *Earth Planet. Sci. Lett.* 236, 899–913, doi:10.1016/j.epsl.2005.06.006.
- Petrenko, V.F., Whitworth, R.W., 1999. *Physics of Ice.* Oxford University Press.
- Ransford, G.A., Finnerty, A.A., Collerson, K.D., 1981. Europa's petrological thermal history. *Nature* 289, 21–24, doi:10.1038/289021a0.
- Raulin, F., McKay, C., Lunine, J., Owen, T.C., 2009. Titan's astrobiology, in: Brown, R.H., Lebreton, J.P., Waite, J.H. (Eds.), *Titan from Cassini-Huygens.* Springer. chapter 9.
- Rempel, A.W., Wettlaufer, J.S., Worster, M.G., 2001. Interfacial premelting and the thermodynamic force: Thermodynamic buoyancy. *Phys. Rev. Lett.* 87, 088501, doi:10.1103/PhysRevLett.87.088501.
- Schmitt, R.W., 1983. The characteristics of salt fingers in a variety of fluid systems, including stellar interiors, liquid metals, oceans, and magmas. *Phys. Fluids* 26, 2373–2377.
- Schmitt, R.W., 1994. Double diffusion in oceanography. *Annu. Rev. Fluid Mech.* 26, 255–285.
- Scott, H.P., Williams, Q., Ryerson, F.J., 2002. Experimental constraints on the chemical evolution of large icy satellites.

- Earth Planet. Sci. Lett. 203, 399–412.
- Seipold, U., Schilling, F.R., 2003. Heat transport in serpentinites. *Tectonophysics* 370, 147–162, doi:10.1016/S0040-1951(03)00183-5.
- Simoës, F., Pfaff, R., Hamelin, M., Klenzing, J., Freudenreich, H., Beghin, C., Berthelier, J.J., Bromund, K., Grard, R., Lebreton, J.P., Martin, S., Rowland, D., Sentman, D., Takahashi, Y., Yair, Y., 2012. Using Schumann resonance measurements for constraining the water abundance on the giant planets—Implications for the Solar System’s formation. *Astrophys. J.* 750, 85, doi:10.1088/0004-637X/750/1/85.
- Sohl, F., Hussmann, H., Schwentker, B., Spohn, T., Lorenz, R.D., 2003. Interior structure models and tidal Love numbers of Titan. *J. Geophys. Res.* 108, 5130, doi:10.1029/2003JE002044.
- Sohl, F., Spohn, T., Breuer, D., Nagel, K., 2002. Implications from Galileo observations on the interior structure and chemistry of the Galilean satellites. *Icarus* 157, 104–119, doi:10.1006/icar.2002.6828.
- Sotin, C., Mitri, G., Rappaport, N.J., Schubert, G., Stevenson, D.J., 2009. Titan’s interior structure, in: Brown, R.H., Lebreton, J.P., Waite, J.H. (Eds.), *Titan from Cassini-Huygens*. Springer. chapter 4.
- Spiegel, E.A., 1972. Convection in stars II. Special effects. *Ann. Rev. Astron. Astrophys.* 10, 261–304.
- Stern, M.E., 1960. The “salt-fountain” and thermohaline convection. *Tellus* 12, 172–175.
- Tobie, G., Gautier, D., Hersant, F., 2012. Titan’s bulk composition constrained by *Cassini-Huygens*: Implication for internal outgassing. *Astrophys. J.* 752, 125, doi:10.1088/0004-637X/752/2/125.
- Tobie, G., Lunine, J.I., Sotin, C., 2006. Episodic outgassing as the origin of atmospheric methane on Titan. *Nature* 440, 61–64, doi:10.1038/nature04497.
- Tobie, G., Mocquet, A., Sotin, C., 2005. Tidal dissipation within large icy satellites: Applications to Europa and Titan. *Icarus* 177, 534–549, doi:10.1016/j.icarus.2005.04.006.
- Travis, B.J., Schubert, G., 2005. Hydrothermal convection in carbonaceous chondrite parent bodies. *Earth Planet. Sci. Lett.* 240, 234–250, doi:10.1016/j.epsl.2005.09.008.
- Tsiganis, K., Gomes, R., Morbidelli, A., Levison, H.F., 2005. Origin of the orbital architecture of the giant planets of the Solar System. *Nature* 435, 459–461, doi:10.1038/nature03539.
- Turner, J.S., 1973. *Buoyancy Effects in Fluids*. Cambridge University Press, New York: New York.
- Turner, J.S., 1974. Double-diffusive phenomena. *Ann. Rev. Fluid Mech.* 6, 37–54.
- Turner, J.S., 1985. Multicomponent convection. *Ann. Rev. Fluid Mech.* 17, 11–44.
- Veronis, G., 1968. Effect of a stabilizing gradient of solute on thermal convection. *J. Fluid Mech.* 34, 315–336.
- Worster, M.G., 2004. Time-dependent fluxes across double-diffusive interfaces. *J. Fluid Mech.* 505, 287–307, doi:10.1017/S0022112004008523.